Proceedings of the
Annual Stability Conference
Structural Stability Research Council
Louisville, Kentucky, April 1-4, 2025

Optimizing the structural performance of extruded aluminum RHS and SHS with internal stiffeners

Juan David Orozco-Sosa[1], Moufahdilou Ouro-Yendou[2],
Carlos Graciano[3], Liya Li[4]

Abstract
This study explores the behavior of optimized extruded aluminum square and rectangular hollow sections (SHS and RHS) with internal stiffeners, applicable in trusses and cross-bracing elements in construction. While current design standards tend to provide conservative resistance predictions for members under combined loads and often overlook aluminum's strength hardening benefits, they can be complex when applied to cross-sections with stiffeners. This conservatism can lead to increased material costs, highlighting the need for more accurate and practical design methods. Therefore, this article numerically analyzes the buckling performance of aluminum RHS and SHS members, using well-defined ABAQUS shell models. Through a detailed parametric study, various elements such as different cross-section geometries, member slenderness, the influence of stiffeners, loading situations, and different aluminum alloys are considered. This approach allows for a precise assessment of the structural behavior of RHS and SHS with stiffeners under various conditions. The results emphasize the potential for optimizing RHS and SHS designs to achieve better performance. Finally, a more economical and accurate design equation is proposed, comparing the ultimate resistance of RHS and SHS obtained in the parametric study with those predicted by existing Canadian design standards CSA S157.

1. Introduction

Since the 1950s, aluminum has been extensively used as a structural material in various applications, particularly in bridges, space structures, and curtain walls (Mazzolani 2004). Aluminum possesses unique properties that set it apart from other construction materials, such as structural steel or stainless steel (see Table 1). Its high strength-to-weight ratio and excellent corrosion resistance, due to the natural formation of a protective oxide layer, eliminate the need for surface treatments. Another key advantage of aluminum is its high malleability, which allows the use of extrusion technology to create complex symmetrical and non-symmetrical cross-sections

[1] Research assistant, Universidad Nacional de Colombia, < judorozcoso@unal.edu.co>
[2] PhD student, Université de Sherbrooke, < moufahdilou.ouro-yendou@usherbrooke.ca>
[3] Full Professor, Universidad Nacional de Colombia, < cagracianog@unal.edu.co>
[4] Assistant Professor, Université de Sherbrooke, <liya.li@usherbrooke.ca>

that are often unachievable with steel. This capability provides designers with immense flexibility in implementing both conventional and unconventional cross-sectional geometries.

However, aluminum alloys are not without limitations. They tend to have a higher cost per kilogram compared to steel, and their modulus of elasticity is only one-third that of steel, making aluminum more susceptible to buckling due to geometric instability.

Table 1: Physical properties of aluminum and structural steel (Beaulieu 2006)

	Aluminum	Structural steel	Stainless steel
Density [kg/m3]	2700	7850	7900
Melting point [°C]	660	1500	1450
Modulus of elasticity [MPa]	70000	200000	200000
Shear modulus [MPa]	27000	77000	77000
Poisson's ratio [-]	0.33	0.30	0.30

Despite these challenges, aluminum rectangular hollow sections (RHS) and square hollow sections (SHS) are widely used in structural applications such as trusses, bracing systems, columns, and beams due to their efficient load-bearing capabilities and aesthetic appeal. These sections provide excellent resistance to bending and torsional effects, making them suitable for lightweight yet robust structural designs. Numerous studies have focused on conventional RHS and SHS for aluminum structural elements under compression, bending, and combined loading, examining a range of aluminum alloys (Faella et al. 2000; Feng and Liu 2019; Feng et al. 2018; Hu et al. 2021; B. Li et al. 2022; Bock et al. 2021).

In contrast, fewer investigations have explored the behavior of complex extruded or stiffened aluminum sections. (Mennink et al. 2005) conducted 40 compression tests on 12 types of complex sections, identifying various geometric instability interactions. (Li 2022) investigated the local buckling behavior of 27 different extruded aluminum sections with complex geometries through extensive numerical simulations, revealing significant conservatism in CSA S157-17 (Canadian Standards Association 2017) predictions and the benefits of adding stiffeners to enhance section resistance. The study highlighted the potential of the Overall Interaction Concept (OIC) as a more accurate and efficient design approach for future aluminum standards. For RHS and SHS, (Su et al. 2016) studied 30 RHS beams with internal cross stiffeners subjected to bending, complemented by 150 numerical models, all classified as Class 1 sections under Eurocode 9. Their results revealed that design codes underestimated the ultimate resistance of aluminum sections.

This paper aims to address these gaps by performing a numerical parametric analysis of the compressive and flexural capacities of various stiffened RHS and SHS, respectively. The study examines four distinct types of stiffeners using advanced numerical models, evaluating their performance against the Canadian design standard CSA S157-17 (Canadian Standards Association 2017). The findings provide valuable insights into the limitations of existing design codes and identify opportunities to enhance their accuracy for complex aluminum sections. In this paper, Section 2 provides a concise overview of the CSA S157 standard and the OIC design method for predicting the behavior of RHS and SHS, both with and without stiffeners. Section 3 describes the development of numerical models, and the finite element (FE) methodology employed and presents the parametric studies, while Section 4 outlines the proposed OIC design equation and compares the numerical results with predictions from various design methods, highlighting their relative accuracy and applicability.

2. Canadian Design Standards CSA S157 and Overall Interaction Concept (O.I.C.)

2.1 Canadian design rule for cross-sections under simple load cases

This section introduces the calculation process for estimating the compressive strength of RHS and SHS made of aluminum alloys, following the provisions of CSA S157 as shown in the Figs. 1 and 2. In general, the compressive resistance C_r is determined by combining the gross cross-sectional area A_g, the normalized buckling stress $\bar{F}$, and the limiting stress F_o. Note that the safety factor ϕ_y is neglected in this study.

The limiting stress F_o is based on the critical condition between local buckling and welding effects. Since welding is not present in the studied sections, local buckling governs the resistance. For RHS and SHS sections, where the buckling plates are supported along both longitudinal edges, F_o is determined as the product of $\sqrt{\bar{F}}$ which reflects the influence of local buckling, and the material's yield strength F_y.

The normalized buckling stress $\bar{F}$ reflects the slenderness of the cross-section and material-specific factors. It depends on the normalized slenderness $\bar{\lambda}$, which is calculated based on the section's geometry and material properties. For heat-treatable aluminum alloys like 6xxx series, a material factor of 0.2 is applied. The section slenderness λ is determined using the width b and thickness t of the most critical flat element supported along its edges. A modification factor m accounts for the interaction between plates, ensuring the slenderness value accurately represents the behavior of the section. For RHS and SHS sections with internal stiffeners, where CSA S157 provides no specific rules, the m-factor recommended by the (Aluminum Association 2020) is applied.

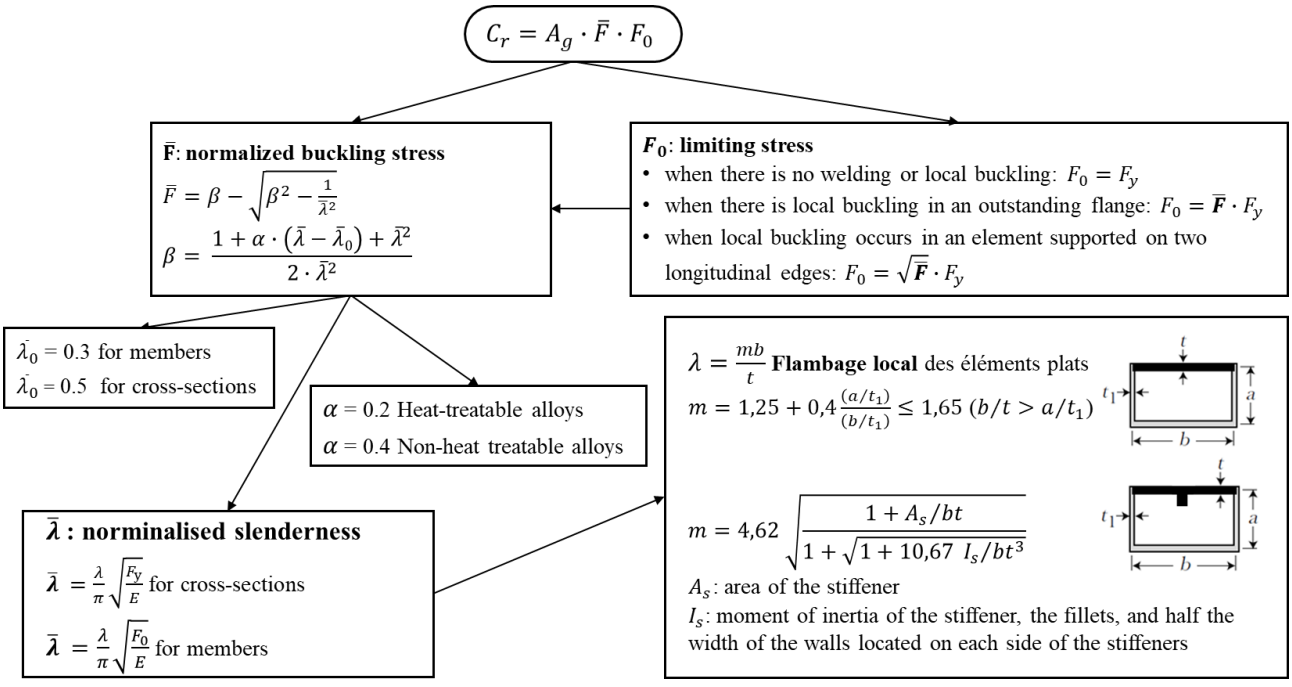

Figure 1: CSA S157 design for aluminum structural elements subjected to compression.

To estimate the bending resistance of aluminum RHS and SHS. CSA S157 classifies cross-sections into three categories: compact (Class 1), non-compact (Class 2), and slender (Class 3). The classification is based on the normalized slenderness $\bar{\lambda}$, which reflects the section's susceptibility to local buckling.

- **Class 1** sections can develop their full plastic moment capacity without being affected by local buckling.
- **Class 2** sections can develop their elastic moment capacity without significant influence from local buckling.
- **Class 3** sections experience plate buckling in compression, and the yield stress is not fully reached.

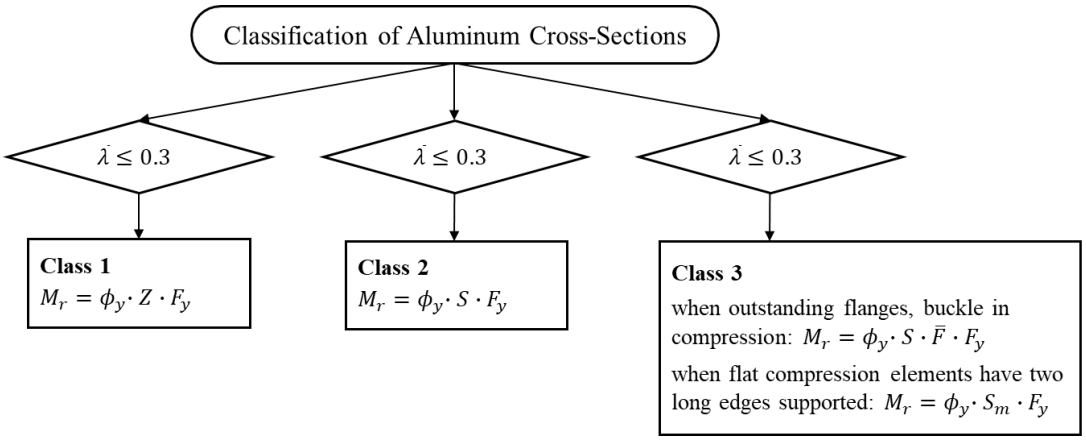

Figure 2: CSA S157 design for aluminum structural elements subjected to bending moment.

The classification is determined using slenderness limits, where the width-to-thickness ratio $\frac{b}{t}$ of the elements is compared to thresholds dependent on material yield strength F_y and a modification factor *m*. The thresholds for each class are expressed as Eq. (1):

$$\begin{cases} \bar{\lambda} \leq 0.3 & \Rightarrow \quad \frac{b}{t} < \frac{250}{m\sqrt{F_y}} & \Rightarrow \text{Class 1} \\ \bar{\lambda} \leq 0.5 & \Rightarrow \quad \frac{b}{t} < \frac{420}{m\sqrt{F_y}} & \Rightarrow \text{Class 2} \\ \bar{\lambda} > 0.5 & \Rightarrow \quad \frac{b}{t} > \frac{420}{m\sqrt{F_y}} & \Rightarrow \text{Class 3} \end{cases} \tag{1}$$

Once the cross-section classification is established, the bending resistance M_r is calculated based on the section's plastic or elastic properties, as defined as Fig. 2, where *Z* is the plastic section modulus of the gross area, *S* is the elastic section modulus. In particular, for the Class 3 RHS and SHS sections, whose flat compression elements have support on both sides, the effective thickness method (ETM) (see Eq. (2)) is applied to calculate the effective elastic section modulus S_m.

$$t_m = t \times \sqrt{\bar{F}} \tag{2}$$

The CSA S157 method for determining the bending resistance of aluminum sections presents several challenges. First, calculating the modification factor *m* becomes increasingly complex for sections with intricate geometries, particularly those featuring internal stiffeners. This adds

significant difficulty when applying the standard to non-traditional or optimized cross-sectional shapes. Second, most of the current design standards, including CSA S157, rely on traditional, manually defined cross-section classification rules. These rules often result in inconsistencies between Class 1 and Class 2 sections, creating discrepancies in the predicted capacities and their practical implications. Lastly, determining the effective elastic section modulus S_m, which accounts for local buckling effects in slender sections, is cumbersome and lacks straightforward guidelines for more complex geometries, further complicating the application of the standard in modern design practices. These limitations highlight the need for updated, more flexible design approaches that can accommodate advanced geometries and reduce inconsistencies in classification and resistance calculations.

2.2 Overall Interaction Concept (O.I.C.)

An alternative design philosophy, known as the OIC, has been developed in recent years to address several of the shortcomings highlighted earlier. The OIC is grounded in the well-established resistance-instability interaction framework and employs a definition of generalized relative slenderness. Unlike traditional methods, it eliminates the need for cross-section classification and the effective thickness approach, instead treating all cross-section shapes uniformly for both sections and members under simple or combined loading scenarios. Initially developed for steel structural elements (Gérard et al. 2021; L. Li et al. 2022; L. Li, Fafard, and Boissonnade 2022; Boissonnade et al. 2017), the OIC has since been adapted to stainless steel (Gagné et al. 2020) and, more recently, extended to aluminum (Dahboul et al. 2023; Tristan 2022).

The OIC introduces a straightforward approach to structural design through the use of $\chi_L = f(\bar{\lambda}_L)$ buckling curves, as illustrated in Fig. 3. These curves incorporate various load ratios, referred to as "*R*-factors." A load ratio is defined as a factor by which an initial set of loads is scaled to reach another specific load level, such as the plastic resistance. For example, the plastic load ratio R_{pl} neglects all instability effects, while the local elastic critical load ratio $R_{cr,L}$ assumes an infinite allowable stress. Both ratios can be calculated using approximate analytical formulae, such as those provided by CSA S157 (Canadian Standards Association 2017), or through more efficient computational tools (Abaqus 2011; Bebiano et al. 2018; Schafer and Ádány 2006) .

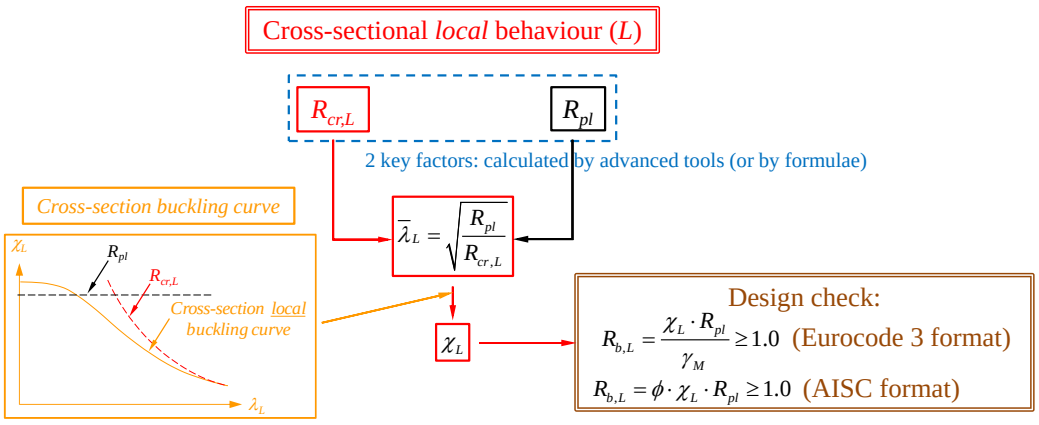

Figure 3: OIC design flow chart for cross-sections

In a manner similar to column flexural buckling, $\bar{\lambda}_L$ represents the cross-section's local relative slenderness. This parameter is used to determine the cross-section's local buckling factor χ_L via

several $\chi_L = f°(\bar{\lambda}_L)$ buckling curves. For a more detailed explanation of the mechanical background underpinning the OIC flowchart, refer to (Boissonnade et al. 2017).

Note that, unlike many current design codes, the final resistance check under the OIC approach involves verifying that the ultimate resistance load ratio $R_{b,L}$ exceeds unity. This ensures that the predicted load-carrying capacity is greater than the applied load, confirming the safety of the design.

3. Numerical investigations

3.1 Basic features and assumptions

Numerical models for rectangular hollow sections under axial compression and combined bending load cases were developed using the non-linear finite element (FE) software ABAQUS (Abaqus 2011). The general-purpose shell element S4R, widely employed in previous numerical studies on aluminum structural elements (Dahboul et al. 2023; Su et al. 2016; Zhao et al. 2019), was used for subsequent Geometrically and Materially Nonlinear with Imperfections Analyses (GMNIA). To achieve an optimal balance between computational efficiency and accuracy, a mesh size equivalent to 1/20th of the average of the web height and flange width was selected.

A quad-linear stress-strain material relationship (Abaqus 2011), converted into true stress and logarithmic plastic strain, was implemented in ABAQUS for both validation and parametric studies. The material behavior of aluminum alloys was characterized using the Ramberg-Osgood equation, modified to account for strain hardening effects and adapted for non-linear analysis in finite element modeling. Key material properties included the yield strength (F_y, defined as 0.2% proof stress), ultimate strength (F_u), and the modulus of elasticity (E), specified as 70,000 MPa in CSA S157. For strain-hardening representation, the exponent n was determined in accordance with Eurocode 9 (European Committee for Standardization 2007). To accurately capture material nonlinearities, stress-strain relationships were developed by assigning 100 data points to each material curve, ensuring reliable predictions in parametric studies. These enhancements effectively account for the unique mechanical properties of aluminum alloys, refining their representation and supporting more accurate structural design applications (Tristan 2022; Dahboul et al. 2023).

As shown in Fig. 4, all models were analyzed under simply supported, fork-type boundary conditions. These conditions restrained the end sections against torsional displacements and out-of-plane displacements along both principal axes, i.e., $u_y = u_z = \theta_x = 0$. At one end, the compression load was applied at a reference point coupled to the end section via rigid body constraints, ensuring uniform load transfer. The longitudinal displacement u_x of the reference point at the opposite end was constrained to prevent axial movement. For the bending load case, moments were directly applied to both reference points, ensuring precise control of the loading conditions.

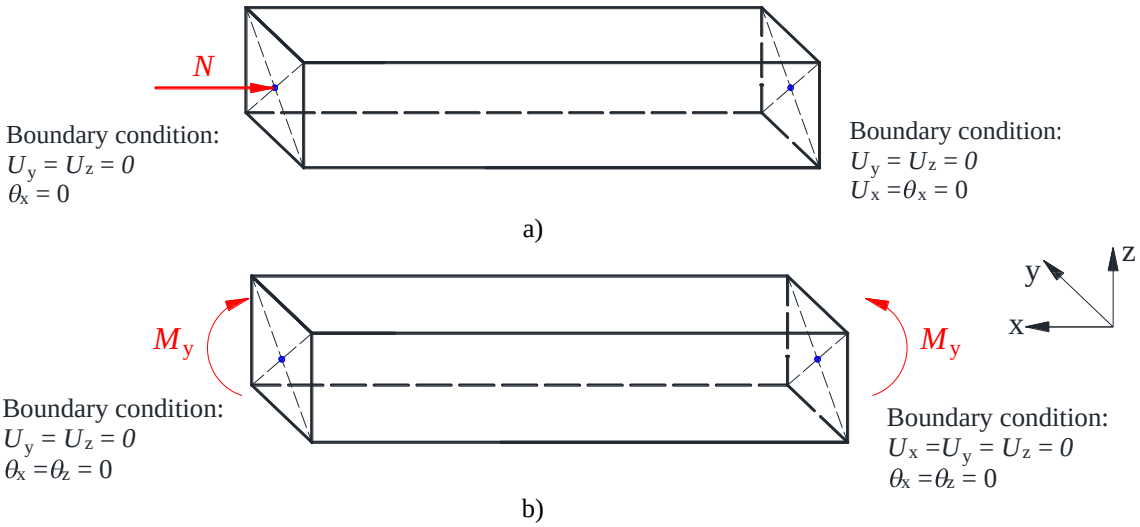

Figure 4: Boundary conditions in numerical models – a) compression load case – b) bending load case.

Previous studies have demonstrated that residual stresses in extruded aluminum structural elements can be considered negligible due to the extrusion manufacturing process of aluminum and the subsequent straightening of the finished member by stretching (Mennink 2002; Mazzolani, et al. 2011). Consequently, no residual stress distribution was implemented in the models. For initial geometrical imperfections, limited experimental measurements have been conducted for aluminum members, and no test data is currently available for RHS and SHS with stiffeners. Therefore, in this study, the first eigenmode from linear buckling analysis (LBA) was adopted to represent the initial imperfection shape. The imperfection amplitude was set as the plate width divided by 200, following common practice in numerical modeling and yields accurate results comparing to the test ones (Dahboul et al. 2024). Additionally, since the focus of this study is on the behavior at the cross-section level, global imperfections were excluded from the model to isolate the effects of local instabilities.

The validation for standardized RHS and SHS has been conducted in (Dahboul et al. 2024), while for RHS and SHS with internal stiffeners, no test data are currently available except for (Su et al. 2016), which, however, is not relevant to the scope of this paper. Consequently, the subsequent numerical studies will be based on the extension of the models validated for standardized RHS and SHS. Further experimental tests are necessary to ensure comprehensive validation and to address the lack of data for sections with internal stiffeners.

3.2 Parametric studies

Extensive parametric studies were conducted to examine the effects of aluminum alloys, section dimensions, stiffener types, section slenderness, and load cases (N or M) on the cross-section resistance of RHS and SHS. The analyses included three aluminum alloys — 6061-T6, 6063-T6, and 6082-T6 — with nominal yield strengths of F_y = 240 MPa, 170 MPa, 260 MPa, respectively, as shown in Fig. 5.

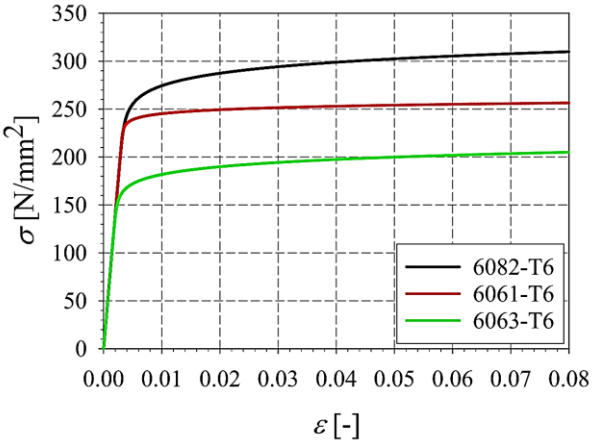

Figure 5: Stress–strain relationships for the various alloys considered.

Various types of RHS and SHS with internal stiffeners (optimised RHS and SHS) were examined in this study, as illustrated in Fig. 6. These sections were designed based on existing standardized RHS and SHS from the catalog (AluQuébec 2021). The widths *a* of the RHS and SHS range from 25.4 mm to 203 mm, heights *b* ranges from 25.4 mm to 406 mm, and the aspect ratios *b/a* vary from 1 to 3. The wall thicknesses range between 1.57 mm and 6.36 mm.

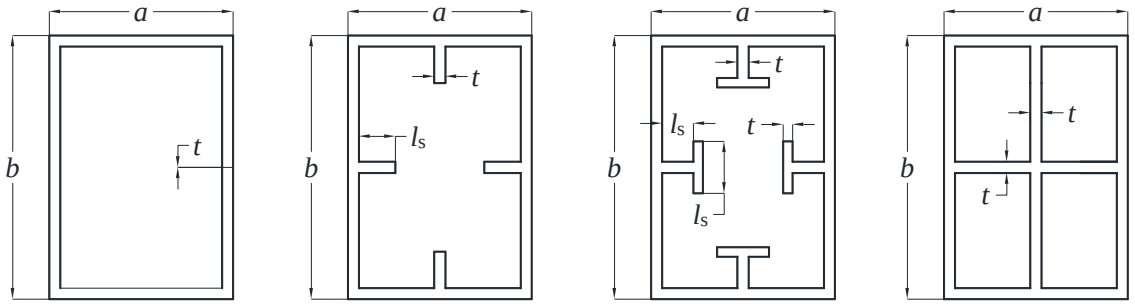

a) b) c) d)

Figure 6: Types of RHS and SHS studied in this paper – a) standardized RHS and SHS – b) Type 1 stiffeners – c) Type 2 stiffeners – d) Type 3 stiffeners

Three innovative types of internal stiffeners were developed to explore various optimization possibilities:

- Type 1: I-shaped stiffeners
- Type 2: T-shaped stiffeners
- Type 3: Cross-shaped stiffeners

Note that in Figs. 6b and 6c, the stiffener lengths l_s were calculated as the average of (*a*-*t*)/10 and (*b*-*t*)/10. The length of the models was set to three times the average of *a* and *b*, providing a balance between minimizing edge effects at the ends of the sections and accounting for the influence of global buckling. In total, 1392 cases were analyzed in this study.

3.3 Influence of stiffeners on the cross-section resistance

Fig. 7 presents all finite element (FE) results for RHS and SHS, both without stiffeners (Fig. 6a) and with stiffeners (Fig. 6b-d), in the OIC $\bar{\lambda}_L$- χ_L format. It is evident that RHS and SHS sections with stiffeners (optimized sections) are significantly more compact compared to standardized RHS

and SHS sections. For the compression load case (Fig. 7a), the normalized slenderness ($\bar{\lambda}_{L,N}$) for standardized RHS and SHS sections can reach up to 1.9, whereas for optimised RHS and SHS sections, the maximum $\bar{\lambda}_L$ is reduced to 1.3. Notably, for sections with Type 2 and Type 3 stiffeners, $\bar{\lambda}_L$ decreases further to approximately 0.9, which is nearly half the value observed for standardized RHS and SHS sections. Additionally, the FE results exhibit significantly less scatter for optimized RHS and SHS sections, particularly for sections with $\bar{\lambda}_L > 1.2$. A similar phenomenon is observed for the bending load case.

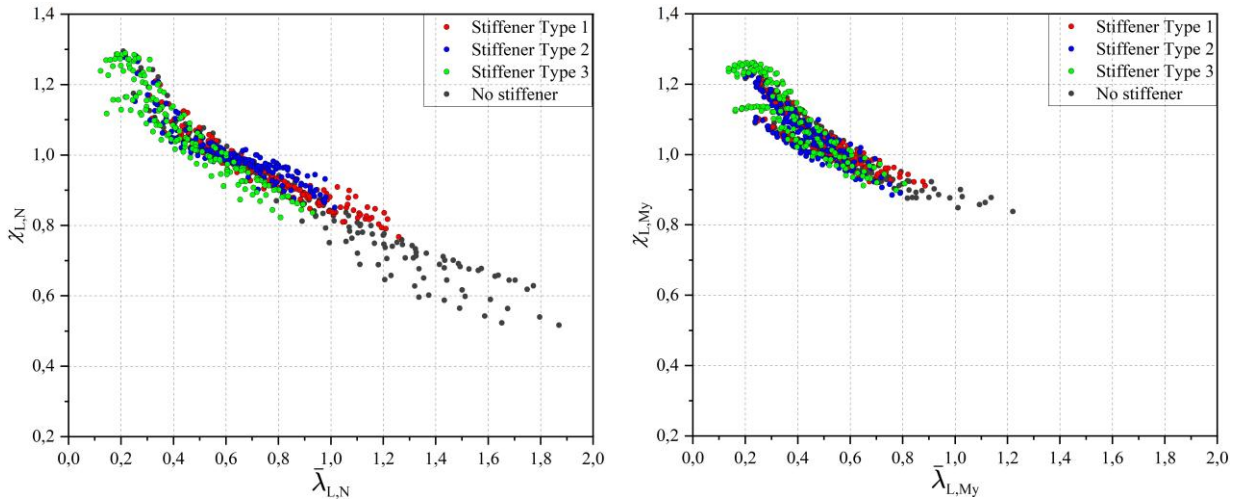

a) b)

Figure 7: FE results for all RHS and SHS sections – a) under compression – b) under bending moment

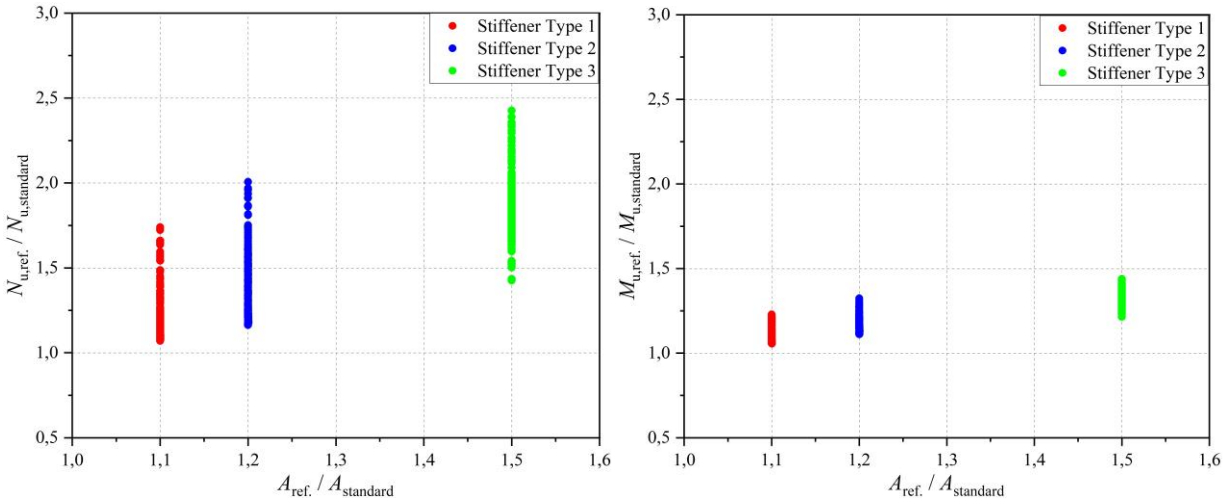

a) b)

Figure 8: Comparison of cross-section resistance and area ratios for different stiffener types comparing to standardized RHS and SHS – a) under compression – b) under bending moment

Fig. 8 presents a comparison of cross-section resistance and area ratios for different stiffener types relative to standardized RHS and SHS sections without stiffeners. Fig. 9 illustrates the same results but as a function of non-dimensional slenderness $\bar{\lambda}_L$. It is observed that, compared to standardized RHS and SHS sections, the cross-sectional area of Type 1 sections increases by approximately 10%, Type 2 sections by about 20%, and Type 3 sections by nearly 50%. Despite this increase in

material usage, the cross-sectional resistance improves significantly due to the stiffeners' ability to reduce local buckling effects.

In general, the cross-sectional resistance gains more compared to standardized RHS and SHS sections as the non-dimensional slenderness $\bar{\lambda}_L$ increases. This is because the stiffeners effectively restrain the development of local buckling, enhancing the overall load-bearing capacity. Among the optimized sections, Type 3 RHS and SHS demonstrate the highest resistance, followed by Type 2, with Type 1 showing the least improvement. For the most slender RHS and SHS sections under compression, the resistance can reach up to 2.5 times that of the standardized cross-section (Type 3), while the corresponding increase in cross-sectional area is only 1.5 times. In contrast, for the bending load case, the improvement in bending resistance is less pronounced than in the compression case, with a maximum increase of approximately 1.5 times. These results show that adding stiffeners may greatly enhances the performance of RHS and SHS sections to varying degrees. However, to achieve an optimal and efficient design, stiffener placement and geometry must be carefully considered to balance material usage and structural performance.

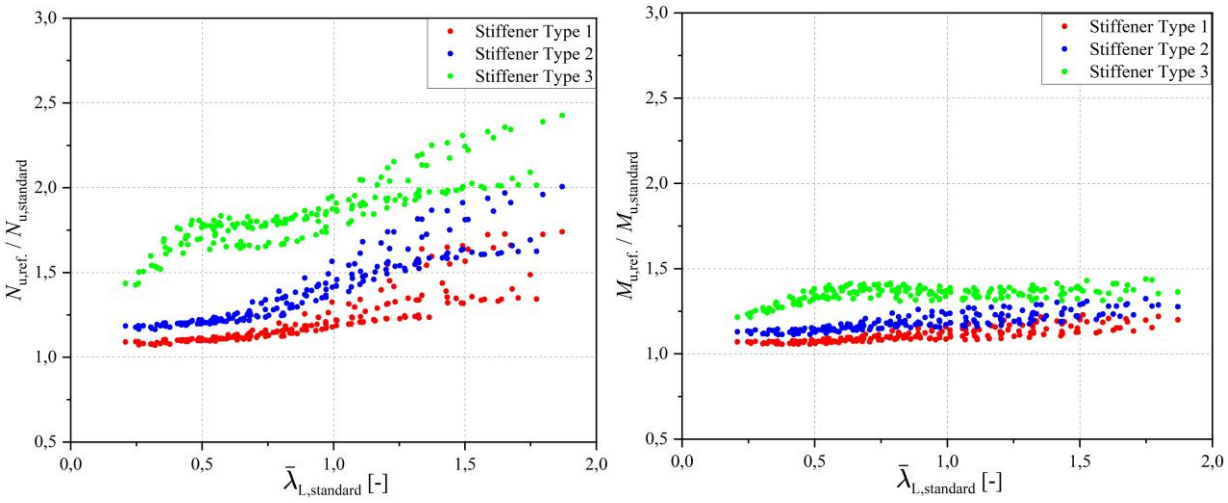

Figure 9: Comparison of cross-section resistance influenced by slenderness for different stiffener types – a) under compression – b) under bending moment

4. Proposed design approach for optimized RHS and SHS sections

The FE results have been used as a reference to develop and evaluate the OIC for optimized RHS and SHS. For standardized RHS and SHS without stiffeners, the OIC-based design methodology is presented in (Dahboul et al. 2024).

As mentioned in Section 2, the OIC method is based on the definition of relative slenderness, denoted here as $\bar{\lambda}_L$ for local (cross-sectional) resistance. This parameter accounts for the balance between plastic resistance and the section's local instability. Once $\bar{\lambda}_L$ is determined, the OIC applies cross-section buckling curves to compute a local penalty factor χ_L (nominalised cross-section resistance), which reduces the plastic resistance due to buckling effects and imperfections. The different steps of this procedure are illustrated in Fig. 3. To derive the OIC $\bar{\lambda}_L$ - χ_L format, two *R*-factors in this study were computed using FE tools. Specifically, ABAQUS was used to determine R_{cr} through LBA (Li 2022) and GMNIA was employed to compute $R_{b,L}$. The plastic

resistance R_{pl} is defined as $R_{pl} = F_y \times A$ for compression and $R_{pl} = F_y \times Z$ for bending. It can also be calculated using Material Nonlinear Analysis (MNA) in ABAQUS.

For all compact optimized RHS and SHS sections with $\bar{\lambda}_L < \lambda_0$ (where λ_0 is a reference limit slenderness), it is observed that the cross-section resistance varies depending on the alloy type. Specifically, optimized RHS and SHS sections made from alloy 6082-T6, which exhibits a stronger strain-hardening effect, achieve higher normalized cross-section resistance χ_L compared to sections made from the other two alloys. Therefore, three distinct design curves were developed based on alloy type. For more slender cross-sections with $\bar{\lambda}_L > \lambda_0$, the proposed design approach follows a more conventional direct $\bar{\lambda}_L$ - χ_L formulation, adopting a modified Ayrton-Perry approach to define the necessary parameters and coefficients. In the proposed equations, α_L represents a general cross-sectional imperfection factor and δ accounts for plate post-buckling effects, as summarized in Table 2.

Table 2: O.I.C. Design proposal for aluminum RHS and SHS with stiffeners under simple load cases

Load Cases	Compression N	Bending M
	For $\bar{\lambda}_{L,N} \leq \lambda_0 = 0.55$:	For $\bar{\lambda}_{L,M} \leq \lambda_0 = 0.48$:
Alloy 6063-T6	$\chi_{L,N} = -0.55\,\bar{\lambda}_{L,N} + 1.3$	$\chi_{L,M} = -0.74\,\bar{\lambda}_{L,M} + 1.36$
Alloy 6061-T6	$\chi_{L,N} = -0.31\,\bar{\lambda}_{L,N} + 1.17$	$\chi_{L,M} = -0.4\,\bar{\lambda}_{L,M} + 1.19$
Alloy 6082-T6	$\chi_{L,N} = -0.82\,\bar{\lambda}_{L,N} + 1.45$	$\chi_{L,M} = -0.92\,\bar{\lambda}_{L,M} + 1.44$
	For $\bar{\lambda}_{L,N} > \lambda_0 = 0.55$:	For $\bar{\lambda}_{L,M} > \lambda_0 = 0.48$:
Ayrton-Perry format	$\Phi_L = 0{,}5 \cdot (1 + \alpha_L \cdot (\bar{\lambda}_{L,N} - \lambda_0) + \bar{\lambda}_{L,N}{}^{\delta})$ $\chi_{L,N} = \frac{1}{\Phi_L + \sqrt{\Phi_L^2 - \bar{\lambda}_{L,N}{}^{\delta}}}$ $\alpha_L = 0.09$ and $\delta = 0.14$	$\Phi_L = 0{,}5 \cdot (1 + \alpha_L \cdot (\bar{\lambda}_{L,M} - \lambda_0) + \bar{\lambda}_{L,M}{}^{\delta})$ $\chi_{L,M} = \frac{1}{\Phi_L + \sqrt{\Phi_L^2 - \bar{\lambda}_{L,M}{}^{\delta}}}$ $\alpha_L = 0.05$ and $\delta = 0.05$

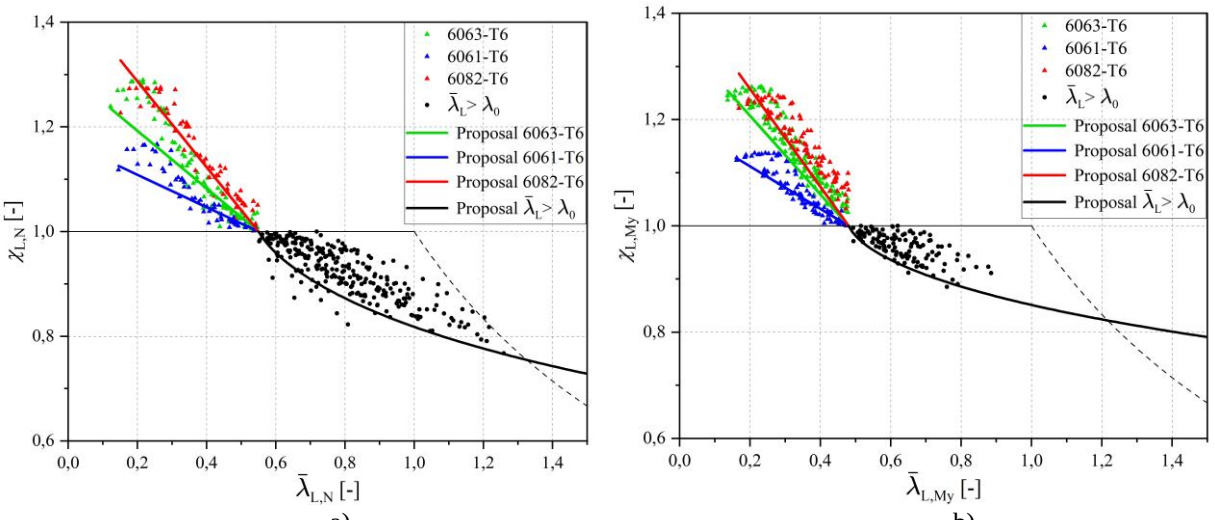

Figure 10: OIC design curves for all RHS and SHS with stiffeners – a) under compression – b) under bending moment

Fig. 10 presents corresponding results covering the entire $\bar{\lambda}_L$ domain, encompassing both compact and slender cross-sections, for compression N and bending M_y. Only one design curve is proposed for compression and one for bending on the safe side. The results demonstrate that the proposed approach provides accurate yet conservative resistance estimates when compared to the reference FE data.

The accuracy of the proposed OIC approach was also evaluated by comparing it against the existing CSA S157 standard as shown in Fig. 11. The reduction factors χ_L, which serve as a direct measure of resistance, were calculated following the recommendations of CSA S157 and then compared to both the proposed OIC approach and the reference FE results. Overall, the comparison demonstrates that:

- The OIC method provides the most accurate and consistent resistance predictions, significantly outperforming the CSA S157 approach.
- CSA S157 design equations tend to yield overly conservative resistance estimates, with predicted resistances sometimes being up to twice as low as the reference FE results, while still maintaining a safe-sided approach.

These findings highlight the superior predictive capability of the OIC method, which balances accuracy and safety more effectively than the existing CSA S157 provisions.

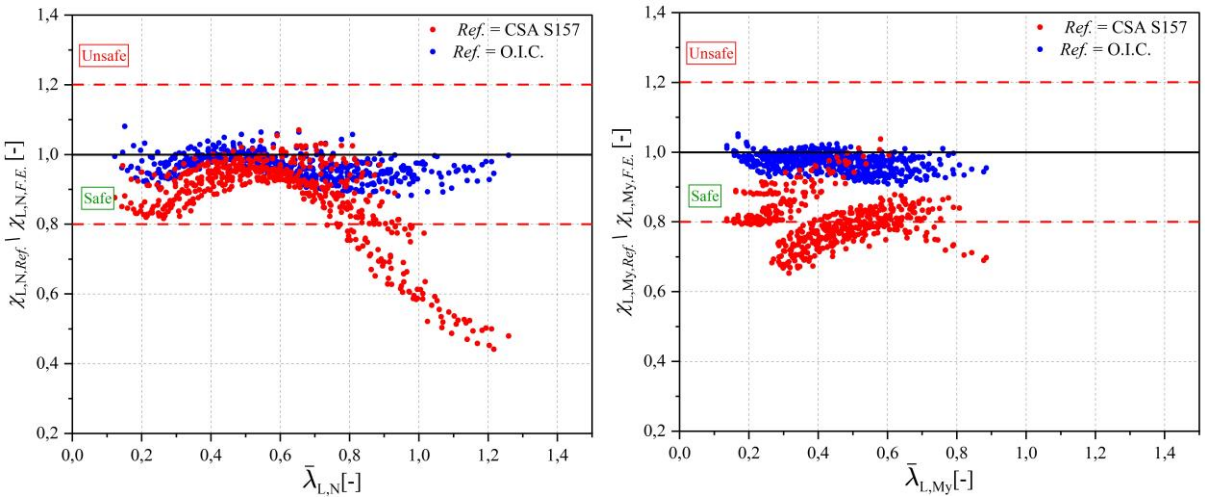

Figure 11: Design rules vs. numerical results for all RHS and SHS with stiffeners – a) under compression – b) under bending moment

Table 3: Statistical results of $\chi_{L,ref.}/\chi_{L,F.E.}$ ratio for all RHS and SHS with stiffeners

Load Cases	Number	Proposal	Mean	COV	Max	Min	< 0.7 [%]	< 0.9 [%]	> 1.10 [%]
All load cases	1044	O.I.C.	0.970	0.031	1.081	0.882	0	1	0
		CSA	0.841	0.125	1.071	0.442	8	66	0
N	522	O.I.C.	0.968	0.035	1.081	0.882	0	3	0
		CSA	0.878	0.139	1.071	0.442	10	42	0
M_y	522	O.I.C.	0.971	0.027	1.052	0.906	0	0	0
		CSA	0.804	0.082	1.038	0.653	6	91	0

In addition, Table 3 provides a detailed statistical analysis of the results across different load cases (*N* or *M*), offering valuable insights into the accuracy and reliability of the proposed OIC approach. Overall, the OIC method exhibits a conservatism of approximately 1% based on the 1044 FE reference cases, with a coefficient of variation (COV) of 3.1%, which is considered excellent given the complexity of the problem. The average values and COV are remarkably consistent, considering the wide range of geometries, aluminum alloys, load cases, and stiffener configurations analyzed in this study. Moreover, the proposed approach demonstrates minimal over-conservatism, with no case exceeding 10% conservatism, ensuring that resistance predictions remain efficient without being excessively restrictive. Additionally, instances of unsafe resistance estimates are limited and can be adequately addressed by applying appropriate safety factors, further reinforcing the practical applicability and reliability of the proposed design framework.

Conclusion

This study has demonstrated the effectiveness of incorporating internal stiffeners in extruded aluminum RHS and SHS to enhance their structural performance. Through an extensive finite FE analysis, it was observed that optimized RHS and SHS with stiffeners exhibit significantly higher resistance compared to standardized sections, particularly for slender cross-sections where local buckling is a governing factor. The proposed OIC-based design method has been validated against 1044 FE results, showing excellent accuracy and consistency. Compared to the existing CSA S157 standard, the OIC approach provides more precise yet safe-sided resistance predictions, overcoming the conservative estimations of current design provisions. Moreover, the study highlighted the influence of aluminum alloy types on cross-sectional resistance, with 6082-T6 exhibiting superior strain-hardening effects. The findings suggest that the proposed design equations offer a more efficient and reliable framework for optimizing the structural design of aluminum hollow sections with internal stiffeners. Future work should focus on experimental validation of the numerical findings, further refinement of design guidelines, and consideration of practical fabrication constraints to ensure broader implementation in engineering practice.

References

Abaqus. 2011. ‘Abaqus 6.11’. *Dassault Systemes Simulia Corporation, Providence, RI, USA*.

Aluminum Association. 2020. *Aluminum Design Manual: 2020*. Washington, D.C.: Aluminum Association.

AluQuébec. 2021. ‘Manuel Des Propriétés Géométriques de Sections Extrudées En Aluminium (Handbook)’. AluQuébec.

Beaulieu, Denis. 2006. *Calcul Des Charpentes d’aluminium*. Les Presses de l’aluminium. Chicoutimi (Québec).

Bebiano, R., D. Camotim, and R. Gonçalves. 2018. ‘GBTul 2.0 − A Second-Generation Code for the GBT-Based Buckling and Vibration Analysis of Thin-Walled Members’. *Thin-Walled Structures* 124 (March):235–57. https://doi.org/10.1016/j.tws.2017.12.002.

Bock, Marina, Marios Theofanous, Samir Dirar, and Nikolaos Lipitkas. 2021. ‘Aluminium SHS and RHS Subjected to Biaxial Bending: Experimental Testing, Modelling and Design Recommendations’. *Engineering Structures* 227 (January):111468. https://doi.org/10/gmtffg.

Boissonnade, Nicolas, Marielle Hayeck, Elsy Saloumi, and Joanna Nseir. 2017. ‘An Overall Interaction Concept for an Alternative Approach to Steel Members Design’. *Journal of Constructional Steel Research* 135 (August):199–212. https://doi.org/10/gbkrf8.

Canadian Standards Association. 2017. *CSA S157-17: Strength Design in Aluminum*.

Dahboul, Sahar, Liya Li, Tristan Coderre, and Nicolas Boissonnade. 2023. ‘5. O.I.C.-Based Design of Extruded and Welded Aluminum I-Sections’. *Structures* 58 (December):105504. https://doi.org/10.1016/j.istruc.2023.105504.

Dahboul, Sahar, Liya Li, Prachi Verma, and Nicolas Boissonnade. 2024. ‘O.I.C.-Based Design of Aluminium Rectangular Hollow Sections under Simple Load Cases’. In . Rio de Janeiro, Brazil.

Dahboul, Sahar, Liya Li, Prachi Verma, Pampa Dey, and Nicolas Boissonnade. 2024. 'O.I.C.-Based Design of Aluminium Rectangular Hollow Sections under Simple Load Cases'. In *10h International Conference on Steel and Aluminium Structures (ICSAS24)*. Rio de Janeiro, Brazil.

European Committee for Standardization. 2007. *Eurocode 9: Design of Aluminium Structures - Part 1-1: General Structural Rules*. Commission of the European Community, Brussels, Belgium.

Faella, C., F. M. Mazzolani, V. Piluso, and G. Rizzano. 2000. 'Local Buckling of Aluminum Members: Testing and Classification'. *Journal of Structural Engineering* 126 (3): 353–60. https://doi.org/10.1061/(ASCE)0733-9445(2000)126:3(353).

Feng, Ran, and Jiarui Liu. 2019. 'Numerical Investigation and Design of Perforated Aluminium Alloy SHS and RHS Columns'. *Engineering Structures* 199 (November):109591. https://doi.org/10/gg3w2w.

Feng, Ran, Wu Zhu, Haiying Wan, Anying Chen, and Yu Chen. 2018. 'Tests of Perforated Aluminium Alloy SHSs and RHSs under Axial Compression'. *Thin-Walled Structures* 130 (September):194–212. https://doi.org/10/gfrr36.

Gagné, Anne-Sophie, Lucile Gérard, and Nicolas Boissonnade. 2020. 'Design of Stainless Steel Cross-Sections for Simple Load Cases with the O.I.C.' *Journal of Constructional Steel Research* 168 (May):105936. https://doi.org/10/gg3w2g.

Gérard, Lucile, Liya Li, Markus Kettler, and Nicolas Boissonnade. 2021. 'Steel I-Sections Resistance under Compression or Bending by the Overall Interaction Concept'. *Journal of Constructional Steel Research* 182 (July):106644. https://doi.org/10.1016/j.jcsr.2021.106644.

Hu, Yaowei, Bin Rong, Ruoyu Zhang, Yichun Zhang, and Song Zhang. 2021. 'Study of Buckling Behavior for 7A04-T6 Aluminum Alloy Rectangular Hollow Columns'. *Thin-Walled Structures* 169 (December):108410. https://doi.org/10.1016/j.tws.2021.108410.

Li, Beibei, Yuanqing Wang, Ying Zhang, Huanxin Yuan, Xinhang Zhi, and Charalampos C. Baniotopoulos. 2022. 'Flexural Behaviour of 7A04-T6 High-Strength Aluminium Alloy SHS and RHS Beams under Moment Gradient'. *Engineering Structures* 259:114138.

Li, Liya. 2022. 'Research Project on the Resistance of Extruded Aluminum Sections with Complex Geometries (Preliminary Studies)'. Research Report for AluQuébec.

Li, Liya, Mario Fafard, and Nicolas Boissonnade. 2022. 'Local and Global Instabilities of Rolled T-Section Columns under Axial Compression'. *Thin-Walled Structures* 178 (September):109517. https://doi.org/10.1016/j.tws.2022.109517.

Li, Liya, Lucile Gérard, Markus Kettler, and Nicolas Boissonnade. 2022. 'The Overall Interaction Concept for the Design of Hot-Rolled and Welded I-Sections under Combined Loading'. *Thin-Walled Structures* 172 (March):108623. https://doi.org/10.1016/j.tws.2021.108623.

Mazzolani, Federico M. 2004. 'Competing Issues for Aluminium Alloys in Structural Engineering'. *Progress in Structural Engineering and Materials* 6 (4): 185–96. https://doi.org/10.1002/pse.178.

Mazzolani, Federico M., Vincenzo Piluso, and Gianvittorio Rizzano. 2011. 'Local Buckling of Aluminum Alloy Angles under Uniform Compression'. *Journal of Structural Engineering* 137 (2): 173–84. https://doi.org/10/chv6cz.

Mennink, J., F. Soetens, and H. H. Snijder. 2005. 'Cross-Sectional Stability of Aluminium Extrusions with Arbitrary Cross-Sectional Shapes-Experimental and Numerical Research'. *Heron* 50 (2): 69–92.

Mennink, Jeroen. 2002. 'Cross-Sectional Stability of Aluminium Extrusions: Prediction of the Actual Local Buckling Behaviour'. https://research.tue.nl/files/2016599/200213965.pdf.

Schafer, B W, and S Ádány. 2006. 'Buckling Analysis of Cold-Formed Steel Members Using CUFSM: Conventional and Constrained Finite Strip Methods'.

Su, Mei-Ni, Ben Young, and Leroy Gardner. 2016. 'Flexural Response of Aluminium Alloy SHS and RHS with Internal Stiffeners'. *Engineering Structures* 121 (August):170–80. https://doi.org/10/f8t9cr.

Tristan, Coderre. 2022. 'Development of an Alternative Design Method for Aluminium Open Cross-Sections Using the Overall Interaction Concept'. MSc Thesis, Quebec City, Canada: Civil and Water Engineering Department, Laval University.

Zhao, Yuanzheng, Ximei Zhai, and Jianhao Wang. 2019. 'Buckling Behaviors and Ultimate Strengths of 6082-T6 Aluminum Alloy Columns under Eccentric Compression–Part I: Experiments and Finite Element Modeling'. *Thin-Walled Structures* 143:106207.